

Genome-wide CRISPR Screening to Identify Drivers of TGF- β -Induced Liver Fibrosis in Human Hepatic Stellate Cells

Shan Yu,* Matthew Ericson, Andrea Fanjul, Derek M. Erion, Maria Paraskevopoulou, Erin N. Smith, Banumathi Cole, Ryan Feaver, Corine Holub, Narender Gavva, Shane R. Horman, and Jie Huang



Cite This: *ACS Chem. Biol.* 2022, 17, 918–929



Read Online

ACCESS |



Metrics & More

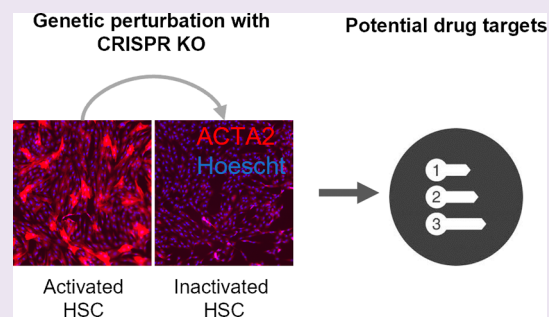


Article Recommendations



Supporting Information

ABSTRACT: Liver fibrosis progression in chronic liver disease leads to cirrhosis, liver failure, or hepatocellular carcinoma and often ends in liver transplantation. Even with an increased understanding of liver fibrogenesis and many attempts to generate therapeutics specifically targeting fibrosis, there is no approved treatment for liver fibrosis. To further understand and characterize the driving mechanisms of liver fibrosis, we developed a high-throughput genome-wide CRISPR/Cas9 screening platform to identify hepatic stellate cell (HSC)-derived mediators of transforming growth factor (TGF)- β -induced liver fibrosis. The functional genomics phenotypic screening platform described here revealed the novel biology of TGF- β -induced fibrogenesis and potential drug targets for liver fibrosis.



INTRODUCTION

Liver fibrosis, one of the advanced stages of chronic liver disease, is a major burden to global health care together with other chronic liver diseases, and the total estimated national hospitalization costs in these patients reached \$81.1 billion from 2012 to 2016.¹ Liver fibrosis is characterized by progressive accumulation of extracellular matrix (ECM) proteins, which distort the physiological architecture of the liver. Currently, there is no approved antifibrotic therapy for reducing the burden of hepatic fibrosis,² as the current standard of care is mainly to target the causative factor. If left untreated, liver fibrosis can develop into hepatocellular carcinoma or result in end-stage liver disease.³

From a pathogenesis perspective, chronic hepatitis B virus/hepatitis C virus infection, rare liver diseases, alcohol abuse, and non-alcoholic steatohepatitis (NASH) can all result in damaged hepatocytes and infiltration of immune cells to the liver, which then activate trans-differentiation of hepatic stellate cells (HSCs) into collagen-producing myofibroblasts. This process can be balanced by counteracting antifibrotic mechanisms, such as HSC inactivation and apoptosis of myofibroblasts or increased fibrinolysis, which lead to scar resolution.⁴ However, if the inflammatory balance is not well controlled and HSCs are continuously activated due to chronic injuries, the myofibroblasts may produce excess quantities of ECM, which destroys the physiological architecture of the liver.⁵

On a molecular basis, transforming growth factor beta (TGF- β), a master profibrogenic cytokine, is synthesized in the form of a latent precursor by non-parenchymal liver cells, such as HSCs, liver sinusoidal endothelial cells, Kupffer cells,

dendritic cells, and natural killer T cells. TGF- β is required to be cleaved by furin-like proteases to become mature but remains biologically inactive due to its association with a protein complex until activated by thrombospondin 1 or some proteases.^{6,7} TGF- β induces HSC activation and trans-differentiation into myofibroblasts, which are associated with loss of intracellular vitamin A droplets, adaptation of fibroblast pathologies, and development of a contractile and migratory phenotype through expression of alpha-smooth muscle actin (α -SMA or ACTA2).⁸ With an increasingly clear role in fibrogenesis, TGF- β represents a promising target for the treatment of liver fibrosis, and several therapeutics have been developed to directly target TGF- β .⁵ However, due to its broad physiological functions, TGF- β inhibition induces undesirable toxicities, which may override its therapeutic benefits.^{9,10} Thus, understanding the pleiotropic effects of TGF- β and its upstream and downstream regulatory mechanisms in HSCs may help reveal druggable nodes in this signaling pathway that are less susceptible to on-target toxicity.

CRISPR/Cas9 has become a popular genetic editing tool due to its ease of use and fewer off-target effects compared to other gene-modulating tools, for example, siRNA technologies.¹¹ CRISPR/Cas9 knockout screens, conducted in both pooled and arrayed formats, have been widely adapted for

Received: January 3, 2022

Accepted: March 2, 2022

Published: March 11, 2022



target identification and mechanistic characterization.¹² While pooled CRISPR/Cas9 screening is typically cheaper and less time-consuming, arrayed CRISPR/Cas9 screening provides more technical flexibility in the types of endpoint functional assays. Moreover, the genotype–phenotype correlation of arrayed CRISPR/Cas9 screening is typically more straightforward and requires less data deconvolution compared to pooled CRISPR approaches.¹³ To understand the pleiotropic effects of TGF- β in HSC-mediated liver fibrogenesis and explore new drug targets for this disease, we performed an arrayed genome-wide CRISPR/Cas9 screen in primary human HSCs using *ACTA2* protein expression as a surrogate readout for HSC activation. We identified an extensive list of regulators with diverse modes of actions, including novel and previously known mechanisms, involved in HSC fibrogenesis. Through a multipronged parallel approach employing differential orthogonal assays, we were able to validate the biological functions of these genetic hits and their relevance in liver fibrogenesis. We demonstrate that the CRISPR/Cas9 knockout screening platform described here has prognostic uses for the identification of biological regulators of HSC activation and potential drug targets for liver fibrosis.

MATERIALS AND METHODS

Human HSC Culture. Human HSCs were purchased from either Lonza (Cat #: HUCL51) or ScienCell (Cat #: 5300) and were cultured according to manufacturers' instructions. Briefly, for cryopreserved HSCs from Lonza, vials of HSCs were taken out of liquid nitrogen storage and were thawed in a water bath. The cells were gently transferred to a conical tube with 5 mL MCST250 medium (Lonza Cat #: MCST250) under sterile conditions. The cell pellet was collected by centrifuging at 250g for 5 min. The cells were then resuspended in MCST250 medium and seeded at a density of 4000 cells/cm² on collagen I coated plates for passage-1 or 8000–10,000 cells/cm² for passage-0. The medium was changed next day to remove any residual DMSO or unattached cells. For cryopreserved HSCs from ScienCell, vials of HSCs were thawed in a water bath and directly seeded into a poly-L-lysine (Cat #: 0413, ScienCell)-coated culture vessel (2 μ g/cm²). The culture medium was refreshed the next day to remove residual DMSO and unattached cells. All cells were cultured in a 37 °C incubator with 5% CO₂. To maintain the HSC culture, we used a complete medium kit (Cat #: 5301, ScienCell). The medium was changed every three days, until the culture was approximately 70% confluent. We did not let cells go beyond 75% confluent because we found overly confluent cells were not able to be trypsinized properly to become single cell suspension resulting in low cell yield. To passage the cells, DPBS was used to wash the cells and then TrypLE express enzyme (Cat #: 12605036, Thermo Fisher Scientific) was added to cover the bottom of culture vessel. The cells were placed into a 37 °C incubator with 5% CO₂ for 3–4 min to allow the cells to detach. When cells were taken out of the incubator, the vessel was tapped on the side to dislodge the cells from the surface, followed by adding complete culture medium. The cell pellet was collected by centrifugation at 160g for 4 min with a breaker set at 5. We seeded cells at 5000 cells/cm² for normal maintenance or passage. A large number of passage-0 cells were obtained from ScienCell and passaged on a large scale and frozen at passage-3 to be used as a screening stock. Before each screen, an appropriate number of cells were thawed and recovered by culturing in tissue culture flasks before being used in CRISPR screen. The number of cell population doublings was critical for these cells because isolated HSCs can be activated spontaneously in primary culture on plastic. Together with other experiments described in this article, the cells between passage-3–6 were used for experiments. 16 h before TGF- β stimulation, culture medium was refreshed with complete medium without FBS. Recombinant human TGF- β 1 protein was purchased from R&D

Systems (Cat #: 240-B-010) and prepared according to manufacturer's instructions.

For small-molecule treatment studies, the cells were seeded on a 384-well plate and cultured overnight to allow them to adhere to the plate. The medium was then replaced with the serum-free medium on the second day to serum starve the cells for 16 h. The compounds were then added to the cells. After 2 h compound treatment, 10 ng/mL TGF- β was added to stimulate the cells for 48 h.

crRNA/tracrRNA/Cas9 Protein Complex Transfection by Electroporation. Briefly, crRNAs (Cat #s can be found on Horizon website by searching the gene names) and tracrRNA (Cat #: U-002005, Horizon) were prepared in Tris–EDTA buffer according to manufacturer's recommendation. For assay development, 10 or 40 μ M crRNA was mixed together with 40 μ M tracrRNA for 20 min to allow crRNA and tracrRNA to anneal. 40 μ M sNLS-SpCas9-sNLS nuclease (Cat #: 9212, Aldelvron) was then added to the crRNA/tracrRNA mix. The added volume for each reagent was described in each individual experiment. The mixture was centrifuged at 500g for 1 min to ensure all solution was collected together, followed by shaking for 30 s to mix. The mixture was then incubated for 15 min to form an RNP complex. During this incubation period, a concentrated single-cell HSC suspension (12,500–50,000 cells/20 μ L) was prepared using either the P3 primary cell 4D-Nucleofector X Kit (Cat #: V4XP-3032, Lonza) or P2 primary cell 4D-Nucleofector X Kit S (Cat #: V4XP-2032, Lonza) according to manufacturer's instructions. Cells were then added to the RNP complex and electroporated using a Lonza 4D-Nucleofector X Unit (Cat #: AAF-1003X). The electroporation programs used were described in each figure description. After 10 min postelectroporation, complete culture medium without antibiotic was then added into each well and gently pipetted up and down. An appropriate amount of mixture was then transferred to a cell culture plate with prewarmed complete medium.

CRISPR Screen Assay Setup and Data Analysis. An appropriate amount of 15 μ M tracrRNA (Cat #: U-002005, Horizon) was prepared in an entire plate of an Abgene 384-well polypropylene storage plate (Cat # AB0781, Thermo Fisher Scientific). 2 μ L/well of 15 μ M tracrRNA was added using a Bravo automated liquid handling system (Cat #: G5563AA, Agilent) to a 384-well electroporation plate (part of P3 primary cell 384-well Nucleofector Kit, Cat #: VSSP-3010), followed by adding 4 μ L/well of 7.5 μ M crRNA from a library source plate. The human genome Edit-R crRNA library was purchased from Horizon (Cat #: GP-005005-E2-025). The electroporation plate was then centrifuged briefly at 500g for 1 min to collect the solutions to the bottom. The plate was shaken on a microplate shaker for 30 s to mix. The mixture was then incubated for 20 min to anneal. 2 μ L/well of 15 μ M sNLS-SpCas9-sNLS nuclease was transferred using a Bravo automated liquid handling system to the electroporation plate. The plate was then centrifuged and mixed to form a RNP complex. During the incubation, 12,500 cells/well HSC single-cell suspension was prepared in 20 μ L P3 buffer in a master mix according to manufacturer's instruction. The cells were then added into RNP complex using an integra 384-well handler and pipetted up and down gently three times to mix. The mixture of cells and the RNP complex in an electroporation plate was then delivered to a 384-well Nucleofector System (Catalog #: AAU-1001) for electroporation using program CA-137. 10 min postelectroporation, 32 μ L of complete culture medium without antibiotic was then added into each well and gently pipetted up and down to mix. 3,000 cells/14.4 μ L from the mixture were then transferred to a cell culture plate (Cat #: 3770, Corning) with 20 μ L prewarmed complete medium.

For the screening data analysis, we used ActivityBase from IDBS. A template used for calculation was generated to allow calculating the percent inhibition of each genetic knockout treatment. The formula to calculate percent inhibition is

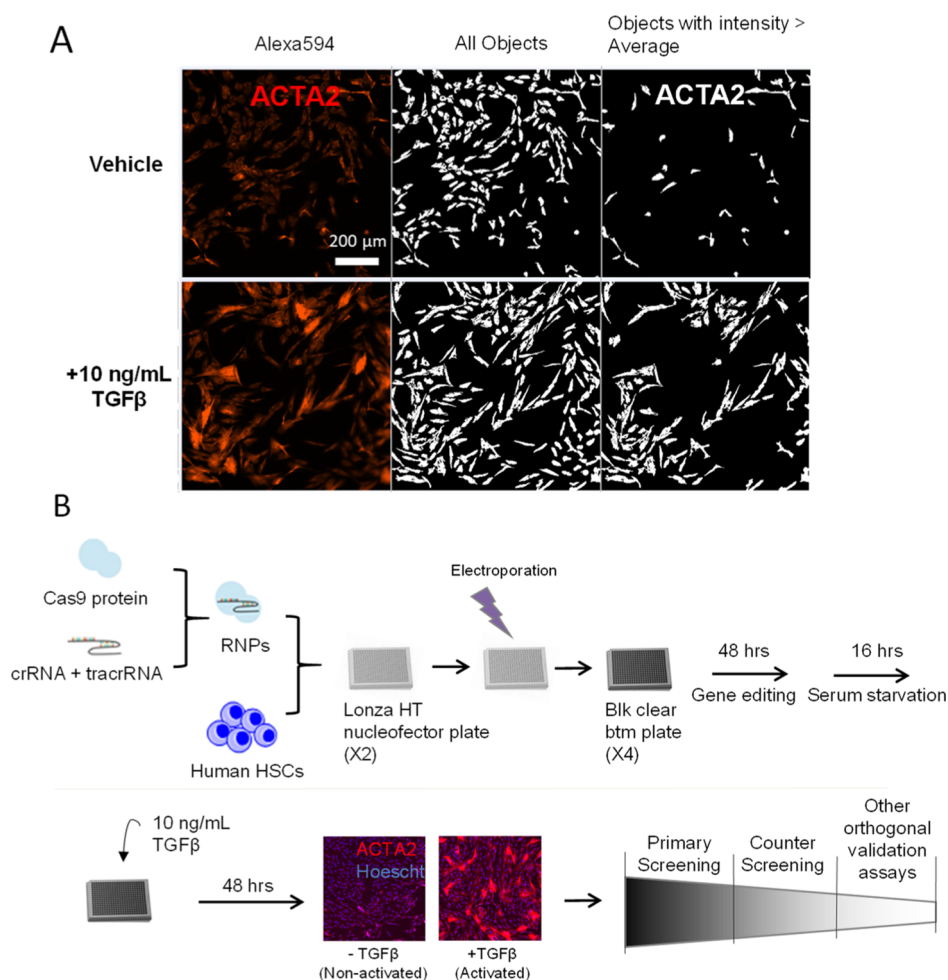


Figure 1. Arrayed CRISPR screen experimental setup using primary human HSCs. (A) Primary human HSCs were plated in a 384-well plate with 3000 cells/well. After 16 h serum starvation, the cells were treated with or without 10 ng/mL TGF- β for 48 h before being fixed and stained with the ACTA2 antibody, followed by a secondary antibody conjugated with Alexa592. Cell images were captured using the ImageXpress Confocal imager, the images were processed by MetaXpress software to show ACTA2-stained raw images (first column), and detected all objects (second column) and objects with intensity above the average intensity in the ACTA2 channel of the vehicle group (third column). (B) CRISPR screen workflow begins with annealing crRNAs with tracrRNA, followed by adding Cas9 protein to form RNPs. The RNPs were electroporated into human HSCs with Lonza HT nucleofector in duplicate. The cells were then transferred into black clear bottom assay plates in duplicate. Thus, each CRISPR library plate is tested in quadruplicate. The cells were then incubated in 37 °C for 48 h to allow CRISPR editing. The cells were serum-starved for 16 h, followed by 10 ng/mL TGF- β stimulation simulation for 48 h. The cells were then fixed and stained with the ACTA2 primary antibody and a secondary antibody, followed by imaging. Upon primary screening completion, the gene hits were tested in a follow-up confirmation screen using the same primary screening assay and a counter screen using the cell viability assay. The confirmed hits were then further filtered through other orthogonal validation assays.

$$\left[\frac{(\text{ACTA2 mean integrated intensity of neg ctrl} - \text{ACTA2 mean integrated intensity of sample})}{(\text{ACTA2 mean integrated intensity of neg ctrl} - \text{ACTA2 mean integrated intensity of pos ctrl})} \right] \times 100$$

This formula yields neg ctrl (non-targeting crRNA)-treated samples having 0% inhibition, while pos ctrl (ACTA2 gRNA)-treated samples having 100% inhibition.

For hit confirmation and validation, the pooled crRNAs for targeting each gene were cherry-picked and reordered from Horizon's human genome Edit-R crRNA library. The crRNAs targeting each gene were tested in a pooled format.

Statistics and Calculations. For all experiments, excluding those from the HemoShear platform, statistical analysis was conducted using the *t*-test or one-way ANOVA with Tukey's post hoc test on Graphpad Prism software with significance of * $p < 0.05$, ** $p < 0.01$, *** $p < 0.001$, and **** $p < 0.0001$. The results are presented as

means \pm SD or means \pm SEM, which is specified in the figure descriptions.

Additional materials and methods are provided in the [Supporting Information](#).

RESULTS AND DISCUSSION

Results. Primary Human Hepatic Stellate Cell CRISPR/Cas9 Screening Assay Development. To develop a robust primary human HSC CRISPR screening platform, we first tested the TGF- β response in primary human HSCs from two different commercial sources (Lonza and ScienCell) by quantifying intracellular ACTA2 protein expression as measured by immunofluorescence staining and high content imaging. ACTA2 expression was significantly upregulated in human primary HSCs by 10 ng/mL TGF- β treatment (Supporting Information, [Figure S1](#)). HSCs from ScienCell demonstrated a more robust response to TGF- β compared to

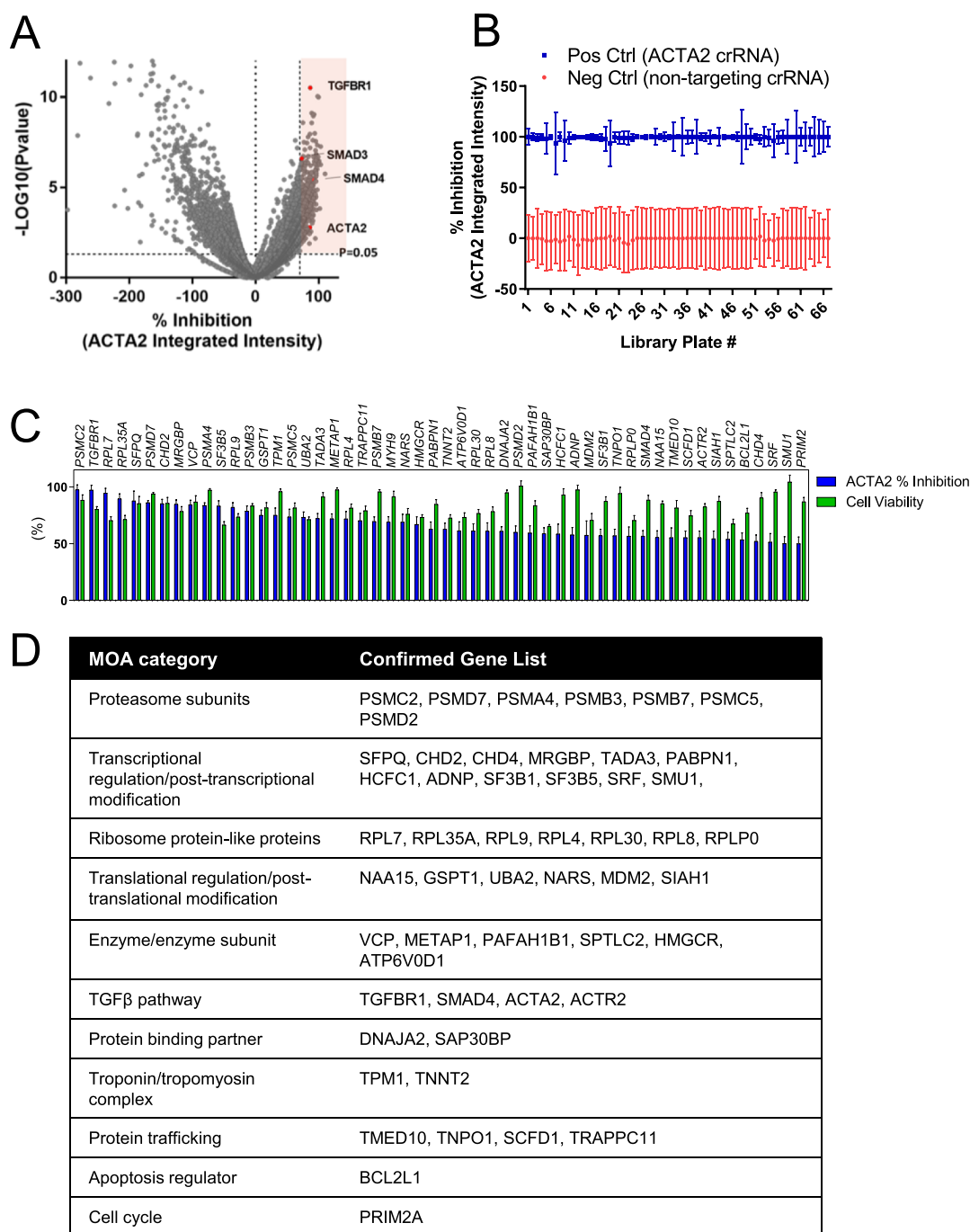


Figure 2. Primary screen and hit confirmation assay results. (A) Volcano plot showed the primary screen results of the percent inhibition of *ACTA2* integrated intensity. Each dot represents a gene knockout treatment. Using a cutoff of 75% *ACTA2* inhibition and 0.05 *P* value, the upper right quadrant showed the 372 gene hits, which were identified from the primary screen. (B) Statistics of *ACTA2*-integrated intensity percent inhibition of positive (*ACTA2* crRNA) and negative (non-targeting crRNA) controls of each screened library plate. Error bar represents standard deviation of the results of positive or negative controls on four assay plates. (C) *ACTA2* expression confirmation and the cell viability results of the CRISPR gene knockout treatments. The cells were treated with CRISPR knockout targeting individual gene as described as Figure 1B. The cell viability was normalized to non-targeting ctrl treated with TGF- β , which was set as 100%. For *ACTA2* percent inhibition results, $n = 14\text{--}23$. For cell viability results, $n = 10\text{--}18$. The error bar represents the standard deviation of each treatment result. (D) Confirmed gene list was further categorized depending on their potential mode of action. Validation of the fibrogenesis effect of CRISPR hits.

HSCs obtained from Lonza (Supporting Information, Figure S1). Therefore, we further optimized our screening assay using the HSCs from ScienCell. To enable CRISPR/Cas9 gene editing in HSCs, we tested multiple electroporation programs in two types of electroporation buffers to deliver ribonucleoprotein (RNP) complexes into HSCs in a high-throughput

384-well screenable format. The results showed that buffer P3 with CA-137 and CM-138 electroporation programs yielded the highest editing efficiency of the *PPIB* control gene (Supporting Information, Figure S2A). To identify positive control CRISPR RNAs (crRNAs) for high-throughput screening, we employed the CRISPR screening process described

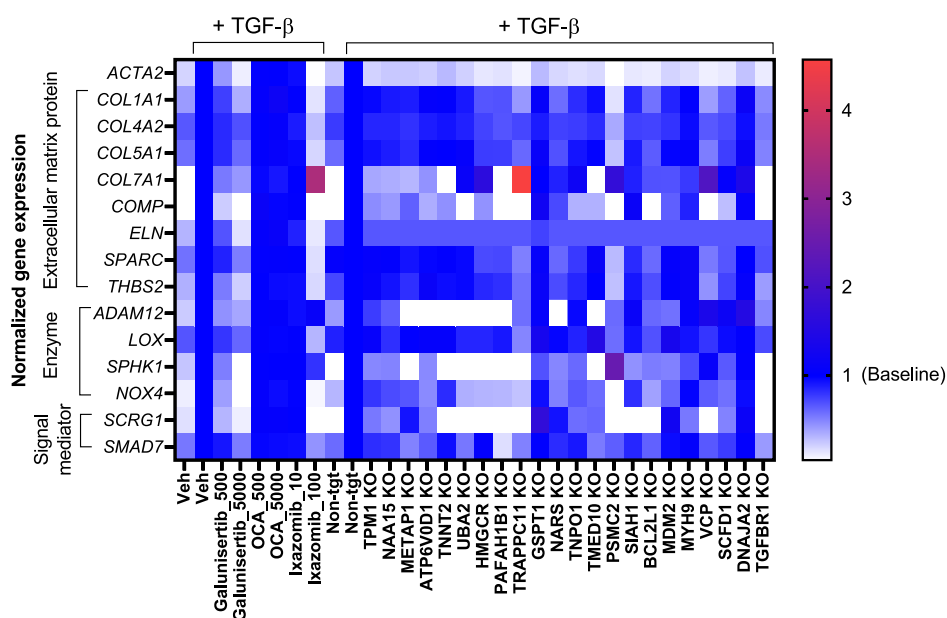


Figure 3. Fibrosis biomarker expression heatmap profile of small-molecule or gene knockout treatment. Human HSCs were either treated with small molecules (500 or 5000 nM galunisertib, 500 or 5000 nM OCA or 10 or 100 nM ixazomib) or genetically knocked out of various genes by CRISPR in combination with or without 10 ng/mL TGF- β . The cell lysates were collected for Nanostring nCounter gene expression panel analysis. The gene expression level of small-molecule treatments was normalized to a small-molecule vehicle with TGF- β treatment, while the gene expression level of CRISPR KO treatments was normalized to non-targeting control with TGF- β treatment with $N = 3$; error bars represent standard deviation.

(Figure 1B) and tested multiple crRNAs for genes that were previously identified to affect the TGF- β signaling pathway.^{14,15} As expected, knocking out *ACTA2* had the most significant effect on the *ACTA2* expression level by reducing its level by 89% (Supporting Information, Figure S2B). Therefore, we chose *ACTA2* crRNAs (a pool of four crRNAs) as the positive control for our functional genomics screen. To further optimize the CRISPR assay, we tested multiple combinatorial conditions, including crRNA and trans-activating crRNA (tracrRNA) concentrations and electroporation cell numbers. We found no significant difference in the efficiency of all four conditions in combination with either cell concentration (Supporting Information, Figure S2C). We moved forward with condition #4 using 25,000 cell/well for electroporation, which uses the least amount of reagents. Next, we determined that 3000 cells/well yielded the best assay window among all three densities (Supporting Information, Figure S2D). Finally, we determined whether there is any significant difference in performance using two high content imaging systems and their associated software; namely the molecular devices ImageXpress confocal and the PerkinElmer Operetta CLS, but we did not see any significant difference in the assay window (Supporting Information, Figure S3). Therefore, we carried out the genome-wide screen on the ImageXpress Confocal platform with robotic assistance.

High-Throughput CRISPR Screen. With the optimized CRISPR assay workflow in place (Figure 1B), the crRNA targeting each gene of the entire annotated genome was tested in duplicate in the electroporation step and further duplicated in the assay plates, which are compatible with the downstream high-content imaging analysis. We screened the entire annotated genome covering 19,027 genes with a commercial crRNA library in a 384-well format (Supporting Information, Figure S4A). The crRNAs, tracrRNA, and Cas9 complexes were delivered using a high-throughput 384-well nucleofection

system. The optimized electroporation program was able to effectively deliver RNPs into the HSCs to edit the control *ACTA2* gene without affecting cell viability (Supporting Information, Figure S4B). For the high-throughput screen, *ACTA2* crRNA and non-target crRNA were included in every assay plate as positive and negative controls, respectively (Supporting Information, Figure S4C and Figure 2B). The assay results were analyzed after each batch with specific quality control (QC) and hit picking criteria. The batch-to-batch variability of *ACTA2* expression was gauged by the difference between the positive (*ACTA2* crRNA treatment) and negative (non-targeting crRNA treatment) controls included in each batch. If the ratio of the average of negative ctrl to positive ctrl of the *ACTA2* expression level was less than 4, suggesting a small assay window, we would move the plate back to the screening queue and not use it for hit picking. This warranted a decent assay window to ensure the reduction of the *ACTA2* level by the testing crRNA was a real signal (Supporting Information, Figure S4D). *ACTA2*-integrated intensity was normalized to the positive and negative controls on each plate, and the percent inhibition of *ACTA2* expression was calculated. Using a threshold of *ACTA2* downregulation of 75% and a significance score (p value) of 0.05, the primary screen identified 372 genes as hits (Figure 2A). Among the hits, there were some genes that were previously known to be involved in TGF- β signaling, including *TGFBR1*, *SMAD3*, and *SMAD4* (Figure 2A), suggesting our CRISPR/Cas9 screening platform was able to identify biologically relevant genes. We further confirmed the effect of these phenotypes in an *ACTA2* downregulation assay and performed cell viability assays to detect any toxicities associated with gene knockdown. Through these triaging efforts, we were able to confirm 52 genes, which yielded greater than 50% *ACTA2* downregulation and greater than 70% cell viability (Figure 2C and Supporting Information, Figure S5). We further categorized these genes based on their

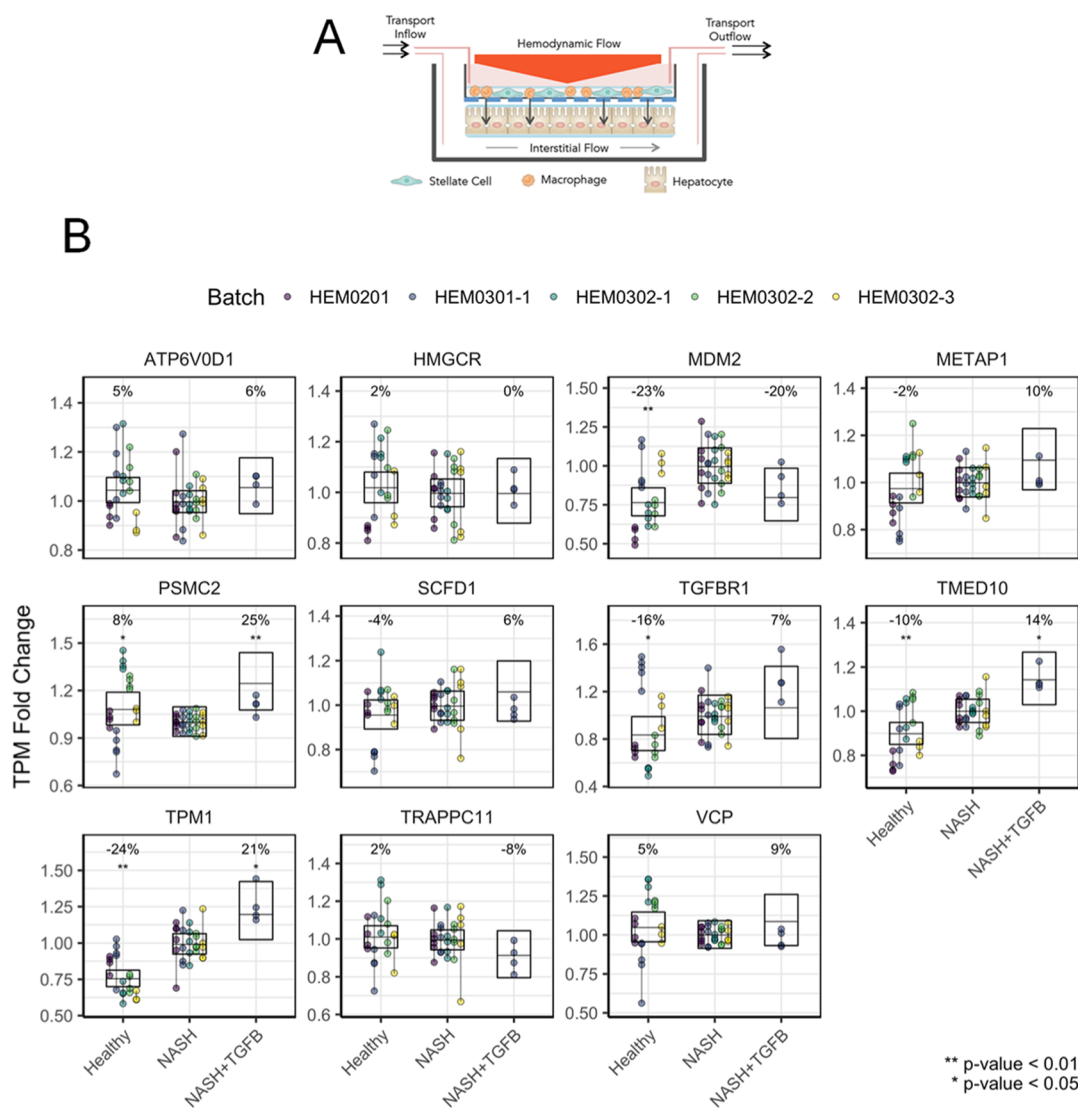


Figure 4. Gene expression level of confirmed hits in an in vitro human liver system of cocultured human hepatocytes and NPCs exposed to hemodynamics under NASH conditions. (A) Using a cone-and-plate viscometer, liver sinusoidal hemodynamics were applied to a transwell multiculture model of primary human NPCs containing stellate cells and macrophages (top of transwell) and primary human hepatocytes (bottom of the transwell). Shear stress is imparted onto the transwell by rotation of the cone (orange triangle). Medium is continually perfused through the inflow and outflow ports to recapitulate interstitial flow. Cells on the device were exposed to media containing a physiological level of factors in healthy or NASH conditions with or without 0.5 ng/mL TGF- β and then collected at the termination of the experiment and analyzed for gene expression via RNA sequencing. Gene expression for NPCs is represented as relative abundance—each gene is normalized to the NASH treatment. Percent changes refer to changes in the across-experiment geometric means; and contrast *p*-values were derived from a linear mixed effect model including treatment as a fixed effect and experiment as a random effect; **p*-value < 0.05, ***p*-value < 0.01; boxes represent the 95% CI of estimated geometric mean across experiments. Five different experiments are represented and *N* = 4–5 for each.

mechanisms of action to bin them according to protein class (Figure 2D).

A number of hits identified from the CRISPR screen demonstrated druggable-like properties. These genes encoded for proteins, which have been predicted to be modulated using conventional pharmacological interventions, such as small molecules and antibodies. We picked these genes to further characterize their effects in ameliorating HSC fibrogenesis. We knocked out these genes individually in HSCs and evaluated how loss of these genes impacted a TGF- β -induced transcriptional profile of a panel of 14 biomarkers previously reported to be associated with liver fibrosis^{16–23} (Figure 3). The TGF- β biomarker panel included canonical ECM proteins, enzymes involved in fibrogenesis, as well as TGF- β signaling mediators. Furthermore, we included two small molecules, galunisertib

and obeticholic acid (OCA), as positive controls. Galunisertib is a TGF- β receptor type I inhibitor and OCA is a FXR agonist, and both small molecules have been investigated experimentally or clinically for treatment of liver fibrosis and other chronic liver diseases (clinical trial for galunisertib: NCT02240433, NCT02178358, and NCT01246986; clinical trial for OCA: NCT03633227 and NCT00570765).^{24–26} The results of these studies showed that galunisertib treatment reduced expression of all 14 biomarkers induced by TGF- β in a dose-dependent manner compared to the vehicle control. OCA did not have any effect on these biomarkers, suggesting OCA might alleviate liver fibrosis through other mechanisms independent of TGF- β signaling, or through a different cell type, such as hepatocytes or Kupffer cells. As our primary screening readout was *ACTA2* intracellular protein expression,

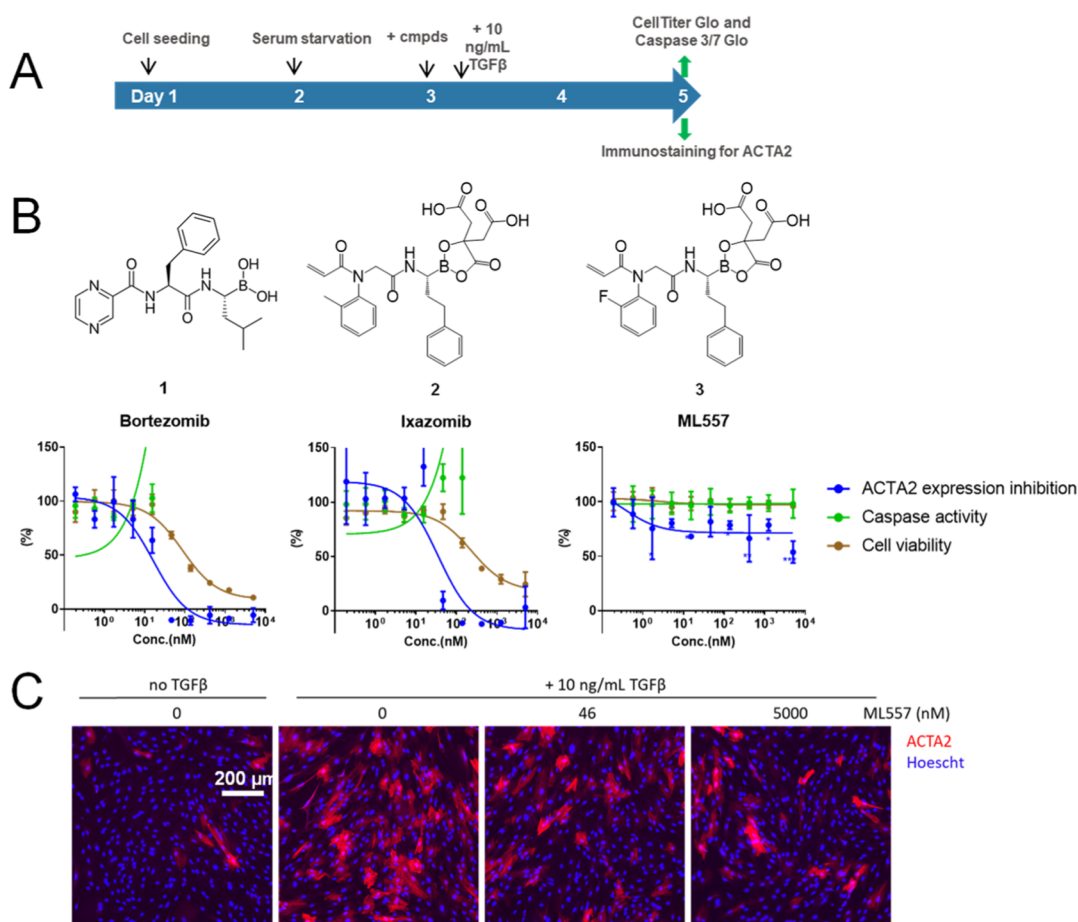


Figure 5. Proteasome subunit target validation with small-molecule tool compounds. (A) Experimental schematic diagram showing compound treatment of human HSCs. 3,000 cells/well were seeded on day 1 in a 384-well plate. The cell culture medium was changed into serum-free medium on the second day 16 h before adding compounds. TGF- β was added to the cells 1 h post small-molecule treatment. After 2 days, the cells were either fixed for ACTA2 immunofluorescence staining or subjected to either CellTiter Glo assay for cell viability or caspase 3/7 Glo assay for caspase activity. (B) Chemical structures and the results of three proteasome inhibitors that were tested in CellTiter Glo, caspase 3/7 activity, and ACTA2 expression inhibition assays. Each assay result was normalized to the vehicle control group with $N = 3$; error bars represent standard deviation. (C) Immunofluorescence images of HSCs that were treated with various doses of ML557 with or without 10 ng/mL TGF- β .

using CRISPR to knockout these hit genes individually also significantly impaired ACTA2 mRNA expression. However, the effects of different CRISPR knockouts on the mRNA expression of other ECM proteins, enzymes, and signaling mediators largely varied (Figure 3). To evaluate each gene's effect on HSC fibrosis, we marked and scored biomarkers by knocking out each of these genes (Supporting Information, Table S1).

In order to understand how the hit genes are regulated in a physiologically relevant liver environment, we interrogated the transcriptome profile of the confirmed hit genes in a complex coculture system pioneered by HemoShear Therapeutics as previously described.²⁷ In this system, we applied liver sinusoidal hemodynamics and interstitial fluid transport parameters to mimic mature, differentiated, and in vivo hepatocyte phenotypes and functions.²⁷ Specifically, primary human non-parenchymal cells (NPCs) including HSCs and macrophages were cocultured with primary human hepatocytes together in an organotypic liver model (Figure 4A). Different conditioned media were used to generate healthy, NASH, and fibrosis liver models as detailed in the Materials and Methods Section. We assessed how hit genes were regulated in this coculture system by RNA-seq transcriptomics. In the NPCs,

MDM2, TGFBR1, TMED10, and TPM1 were significantly elevated in the NASH liver model compared to a healthy liver model. PSMC2, TMED10, and TPM1 were significantly increased in the fibrosis model (the NASH model stimulated with TGF- β) compared to the unstimulated NASH group (Figure 4B). These results suggest that hit genes expressed in the NPCs might play a role in the pathogenesis of NASH and its progression into fibrosis. To understand how the expression levels of these hit genes are changed specifically in the HSC compartment, we analyzed publicly available transcriptomic datasets published in the GEO Profiles database (Supporting Information, Table S2). In two microarray studies GSE68000²⁸ and GSE67664,²⁸ quiescent HSCs (qHSCs) were passaged multiple times to obtain an activated HSC (aHSC) phenotype, while in the RNA-seq study GSE68108, the qHSCs were serum-starved for 48 h before stimulating with TGF- β for 16 h to activate the cells. The fold change of each hit gene in aHSCs from the public transcriptomic studies was provided if the genes were significantly differentially expressed (see methods for microarrays and RNA-Seq data analysis). Indeed, TPM1 and TGFBR1 levels were upregulated more than 1.5-fold in aHSCs in these studies (Supporting Information, Table S2), further supporting the potential

regulatory effects of our hit genes in HSCs during the pathogenesis of liver fibrosis.

Among the confirmed hit genes, we were intrigued by the suppression effect of multiple fibrosis biomarkers in human HSCs through the disruption of the *PSMC2* gene, which encodes 26S protease regulatory subunit 7, a proteasome subunit. As Takeda has developed a series of proteasome inhibitors for treating cancers, Velcade (bortezomib) and Ninlaro (ixazomib), we next tested whether suppressing proteasome activity by proteasome inhibitor drugs alleviates the fibrosis phenotype in human HSCs. We treated human HSCs with three small-molecule analogs, including bortezomib, ixazomib, and ML557 (Figure 5B). After 48 h of TGF- β stimulation, cells were either fixed for *ACTA2* immunostaining or lysed for caspase activity or cell viability assessment (Figure 5A). We observed that HSCs treated with all three analogues reduced the *ACTA2* protein expression level as measured by immunofluorescent imaging. However, *ACTA2* reduction by bortezomib and ixazomib was also accompanied by reduced cell viability decreased and increased caspase. Interestingly, ML557 was able to significantly reduce the *ACTA2* protein level in a dose-dependent manner without increasing caspase activity or causing cell death (Figure 5B,C). These data suggest that inhibiting proteasome activity with small molecules may resolve TGF- β -induced HSC activation.

In order to develop specific targeting strategies and understand the potential on-target off-tissue side-effects of these target genes, we evaluated the cell type-specific expression pattern of these genes by curating our internal mouse liver bacterial artificial chromosome translating ribosome affinity purification (bacTRAP) dataset. BacTRAP is an in vivo methodology that readily and reproducibly identifies translated mRNAs in any cell type of interest. This technique involves expression of an EGFP-L10a fusion protein in bacTRAP transgenic mice, which enables tagging of polyribosomes for immunoaffinity purification of mRNAs in specific cell types of interest.²⁹ In our bacTRAP study, we used an *ACTA2* promoter-driven bacTRAP mouse line to specifically profile their translating mRNAs in HSCs. We treated these mice with either a vehicle control or carbon tetrachloride (CCl_4) to induce liver fibrosis, then collected mouse liver samples and conducted TRAP experiments to profile the translating mRNAs in the HSCs at the moment of sample collection. The RNA expression levels in the HSCs (immunoprecipitated or IP) were compared to those in the total liver tissue to understand whether hit genes were expressed more specifically within the HSC compartment. In particular, *Mdm2*, *Myh9*, *Tgfb1*, *Tnnt2*, and *Tpm1* mRNA levels were significantly higher in the HSCs compared to the whole liver in the vehicle-treated group; while *Myh9*, *Siah1a*, *Tgfb1*, *Tnnt2*, and *Tpm1* mRNA levels were significantly higher in HSCs compared to the whole liver in the CCl_4 -treated group (Supporting Information, Figure S6). These results indicate that these hit genes were enriched specifically in HSCs under normal or CCl_4 -induced liver fibrosis condition.

To understand whether genetic variation in these genes was associated with biomarkers of liver disease in humans, we performed genome-wide association of the AST to platelet ratio index (APRI) and the NAFLD fibrosis score (NFS) in the UK Biobank. To assess gene-level association, we used multimarker analysis of GenoMic annotation (MAGMA) (PMID: 25885710) and identified genome-wide significant

gene-level associations ($P < 2.8 \times 10^{-6}$) with *TPM1*, *METAP1*, *PSMB7*, *PSMD2*, *TNPO1*, and *BCL2L1* with APRI; and *TPM1*, *HMGCR*, *PSMD2*, and *BCL2L1* with NFS (Table 1). These results indicate that genetic variation in these genes may impact biomarkers of NASH and liver fibrosis.

Table 1. Association of the Confirmed Hit Genes with AST to the Platelet Ratio Index (APRI) and Liver Fibrosis Phenotype^a

| gene name | APRI MAGMA | fibrosis score MAGMA |
|-----------------|--|--|
| <i>PSMC2</i> | 2.25×10^{-3} | 2.07×10^{-2} |
| <i>TGFBR1</i> | 2.09×10^{-1} | 5.09×10^{-1} |
| <i>SFPQ</i> | 2.27×10^{-1} | 4.70×10^{-1} |
| <i>PSMD7</i> | 4.64×10^{-2} | 4.93×10^{-1} |
| <i>CHD2</i> | 2.37×10^{-2} | 5.54×10^{-1} |
| <i>MRGBP</i> | 1.81×10^{-1} | 4.15×10^{-1} |
| <i>VCP</i> | 1.50×10^{-3} | 5.50×10^{-1} |
| <i>PSMA4</i> | 1.39×10^{-1} | 3.41×10^{-3} |
| <i>GSPT1</i> | 2.00×10^{-1} | 4.63×10^{-3} |
| <i>TPM1</i> | 1.44×10^{-17} | 1.13×10^{-14} |
| <i>PSMC5</i> | 2.31×10^{-2} | 1.75×10^{-1} |
| <i>UBA2</i> | 5.35×10^{-1} | 6.24×10^{-2} |
| <i>TADA3</i> | 1.81×10^{-1} | 5.23×10^{-1} |
| <i>METAP1</i> | 7.86×10^{-15} | 1.78×10^{-4} |
| <i>TRAPPC11</i> | 2.21×10^{-1} | 1.70×10^{-1} |
| <i>PSMB7</i> | 2.74×10^{-7} | 6.87×10^{-2} |
| <i>NARS</i> | 5.01×10^{-3} | 7.05×10^{-1} |
| <i>HMGCR</i> | 1.07×10^{-3} | 1.86×10^{-12} |
| <i>PABPN1</i> | 7.00×10^{-2} | 3.58×10^{-1} |
| <i>TNNT2</i> | 3.70×10^{-2} | 1.48×10^{-1} |
| <i>ATP6V0D1</i> | 3.46×10^{-4} | 4.81×10^{-1} |
| <i>DNAJA2</i> | 1.01×10^{-1} | 2.01×10^{-3} |
| <i>PSMD2</i> | 2.06×10^{-11} | 4.20×10^{-14} |
| <i>PAFAH1B1</i> | 1.01×10^{-2} | 7.70×10^{-4} |
| <i>ADNP</i> | 8.52×10^{-1} | 5.04×10^{-2} |
| <i>MDM2</i> | 2.88×10^{-1} | 6.67×10^{-1} |
| <i>SF3B1</i> | 1.38×10^{-2} | 1.02×10^{-5} |
| <i>TNPO1</i> | 9.14×10^{-12} | 1.81×10^{-5} |
| <i>SMAD4</i> | 9.64×10^{-1} | 7.12×10^{-2} |
| <i>NAA15</i> | 4.49×10^{-1} | 2.45×10^{-1} |
| <i>TMED10</i> | 1.31×10^{-1} | 2.85×10^{-1} |
| <i>SCFD1</i> | 1.13×10^{-1} | 6.85×10^{-1} |
| <i>SIAH1</i> | 1.14×10^{-1} | 1.92×10^{-1} |
| <i>BCL2L1</i> | 2.87×10^{-14} | 8.52×10^{-22} |
| <i>CHD4</i> | 2.97×10^{-1} | 7.17×10^{-1} |
| <i>SRF</i> | 5.70×10^{-1} | 7.10×10^{-1} |
| <i>SMU1</i> | 2.98×10^{-4} | 1.57×10^{-2} |

^aThe MAGMA package was used to identify genes with a significant effect (P value $< 2.818 \times 10^{-6}$, bolded numbers) on APRI and NAFLD fibrosis scores in the UK Biobank. APRI, used to estimate prevalence of cirrhosis, was calculated as (AST/33)/platelet count X 100. The NAFLD fibrosis score was calculated from a linear model based on age, BMI, AST/ALT, albumin, platelet count, and the presence of diabetes.

Finally, we consolidated all the accumulated data for these targets to rank them according to their relative importance in the pathogenesis of HSC-mediated liver fibrosis. In summary, we performed experiments to knockout potential target genes using CRISPR/Cas9 and evaluated the intracellular *ACTA2* protein level (Figure 2C), cell viability (Figure 2C), and liver fibrosis biomarkers (Figure 3). We analyzed the RNA

Table 2. Summary Table of Hit Confirmation and Validation Test Results^a

| gene | CRISPR KO | | | RNA differential expression | | cell type specific expression | human genetics | total number of * |
|-----------------|------------------------------|----------------------------|---------------------------------|---|----------------------|-------------------------------|------------------------|-------------------|
| | ACTA2 expression (Figure 2C) | cell viability (Figure 2C) | biomarker expression (Figure 3) | public transcriptome profile (sup Table S2) | HemoShear (Figure 4) | BacTRAP (Sup Figure S6) | U.K. BioBank (Table 1) | |
| <i>TPM1</i> | *** | *** | * | *** | *** | ** | *** | 18 |
| <i>PSMC2</i> | *** | *** | *** | * | ** | * | * | 14 |
| <i>VCP</i> | *** | *** | *** | * | * | * | * | 13 |
| <i>METAP1</i> | *** | *** | ** | * | * | * | ** | 13 |
| <i>HMGCR</i> | ** | ** | *** | ** | * | * | ** | 13 |
| <i>SCFD1</i> | ** | ** | *** | ** | * | * | * | 12 |
| <i>TRAPPC11</i> | *** | ** | *** | * | * | * | * | 12 |
| <i>TMED10</i> | ** | ** | ** | * | *** | * | * | 12 |
| <i>MDM2</i> | ** | ** | * | ** | ** | * | * | 11 |
| <i>ATP6V0D1</i> | ** | ** | ** | * | * | * | * | 10 |

^a*Data do not support hypothesis; **some data might support hypothesis; and ***strong data support hypothesis. The result of each assay was evaluated depending on whether strong data supported the hypothesis (***), some data might support hypothesis (**), or no data supported the hypothesis (*).

differential expression levels in human HSCs in both published transcriptome datasets (Supporting Information, Table S2) and the HemoShear organotypic coculture platform (Figure 4). For further disease relevance, we evaluated HSC cell type-specific expression in a mouse liver fibrosis bacTRAP experiment (Supporting Information, Figure S6). To associate any genetic variants with traits linked to liver fibrosis, we also performed MAGMA analyses on the UK Biobank database (Table 1). We summarized the results of these studies and scored each target gene depending on whether the individual experimental results supported the hypothesis that the gene could be a potential drug target for liver fibrosis. A higher score suggested more evidence from validation studies supported a gene could be a potential target for liver fibrosis (Table 2). In summary, we have demonstrated the value of CRISPR/Cas9 high-content screening for identifying potential genetic targets in HSCs for liver fibrosis and described a parallel workflow of validation experiments that can be employed to triage and rank potential targets for preclinical drug discovery efforts.

Discussion. Chronic liver diseases are a major global health burden and account for approximately 2 million deaths per year worldwide. In the liver, development of fibrosis has a significant impact on prognosis as well as quality of life.^{30,31} The medical burden associated with liver fibrosis has significantly increased over the years, as exemplified by the rapidly increasing inpatient health care utilization. The total estimated U.S. national hospitalization costs in patients with chronic liver disease from 2012 to 2016 reached \$81.8 billion.¹ The development of liver fibrosis is known to be associated with numerous secondary complications, including ascites, hepatic encephalopathy, hepatorenal syndrome, portal hypertension, and variceal bleeding. When liver fibrosis is left untreated, the disease develops into a more advanced stage such as hepatocellular carcinoma, which has an even lower transplant-free survival rate.³² With the emergence of the COVID-19 pandemic, the presence of chronic inflammatory diseases, such as liver fibrosis, results in an even poorer outcome in COVID-19 patients, including increased risk for mechanical ventilation, development of acute kidney injury, and higher mortality rates.^{33,34} Although therapeutic targets and remedies have been extensively explored, currently there are no approved therapies for treating liver fibrosis. Here, we

present a genome-wide approach to interrogate potential therapeutic targets for liver fibrosis using the CRISPR technology on a high-throughput scale.

From a drug discovery perspective, compared to small-molecule phenotypic screen, using CRISPR/Cas9 to ablate individual genes to study their biological functions under specific disease conditions is desirable because it provides direct information regarding potential genes involved in disease biology. Alternatively, small-molecule phenotypic screens typically require extensive target deconvolution to discriminate compound activities and efficacies. Herein, we showed that the CRISPR/Cas9 high-throughput screening approach can identify both key regulators of liver fibrosis as reported in the literature (e.g., *TGFBRI*, *SMAD3*, and *SMAD4*) and novel genes that demonstrate yet-to-be-reported functions. That being said, to be pursued as a drug target many properties of a gene/protein need to be assessed, including but not limited to its genomic association with disease, functions in regulating disease, safety concerns, and druggability. A genetic hit list identified in a CRISPR/Cas9 genome-wide screen yields a pragmatic starting point for target identification and validation studies. In the genomic screening project described here, we followed up the primary high-throughput screen with a series of orthogonal assays designed to validate the biological functions of hit targets both in vitro and in vivo. In order to corroborate the clinical translatability of lead targets, we also interrogated their potential association with NASH and liver fibrosis by curating clinical human data (UK Biobank). Considering the preponderance of known liver fibrosis-modifying genes that were scored in our screen, we demonstrated that such functional genomics approaches are able to yield clinically relevant genetic targets.

Among the top targets that we identified, quite a few have literature-based evidence of their roles in the pathogenesis of hepatic fibrosis. For example, tropomyosin-1 (encoded by *TPM1*), as one of the hits, was reported to be correlated with increased levels of α -SMA during liver injury in animal models as well as human cirrhotic livers.³⁵ It was associated with cell motility and contractility and was used as a biomarker for HSC activation and liver tissue ECM remodeling.^{36,37} 3-Hydroxy-3-methylglutaryl-CoA reductase (encoded by *HMGCR*), the target of statins, a class of drugs that were

used for treating high cholesterol-induced metabolic diseases, was also identified in our screen as one of the top targets. Although statins are not approved by the FDA for treating liver fibrosis, numerous literature reported the role of *HMGCR* in the regulation of liver inflammation and hepatic portal hypertension, which are the key components that contribute to the hepatic fibrosis progression.³⁸ The use of statins was associated with the lower prevalence of advanced liver fibrosis in patients with type 2 diabetes.³⁹ This evidence suggests the potential of statins as a class of drugs and *HMGCR* as a target for therapeutic development for patients with liver fibrosis.

Importantly, some therapeutic targets that have been reported in the literature to contribute to liver fibrosis were not identified as hits in our CRISPR screen. Some potential non-technical reasons for this observation could be (1) these genes are involved in essential biological functions, and complete loss-of-function of these genes resulted in cytotoxicity or (2) our assay setup and readout using *ACTA2* could be limited in identifying other classes of targets outside of TGF- β signaling, which affect liver fibrosis. For example, platelet-derived growth factor receptors (PDGFRs) have been described in regulating HSC activation and hepatic fibrosis.⁴⁰ However, the pathways of PDGFRs do not converge with TGF- β signaling, and knocking out genes that encode PDGFR proteins did not reduce TGF- β -induced HSC activation. To address these potential screening biases, multiple readouts or an unbiased readout, such as cell painting morphological profiling,⁴¹ instead of a single biomarker, could be used in future studies to identify a broader range of targets with more diverse modes of action.

To triage hits from the primary CRISPR screen, we used multiple orthogonal assays to validate their antifibrosis functions and constructed a method to rank them and enable additional downstream prioritization and confirmation studies. Myriad target ranking systems have been reported for various diseases,^{42–45} where each ranking system incorporates different experimental elements for its analysis pipeline. The most common elements of these systems include biological function, genetics, safety, and druggability, which we evaluated in our target prioritization analyses. Depending on the sets of data to be included in the analysis and type of analytical method to be used, the target ranking could potentially be changed. Further studies on the validation and preclinical drug development of the targets described here are therefore warranted.

SIGNIFICANCE

In summary, we have developed a new cell-based phenotypic screening method that invokes primary human HSC culture to create a physiologically relevant model system of liver fibrosis. This screening and validation pipeline allowed us to interrogate the role of the entire annotated genome in HSC activation and liver fibrosis. The target list yielded from this liver fibrosis industrial drug discovery platform may provide further insights and opportunities for developing next-generation therapies for liver fibrosis.

ASSOCIATED CONTENT

Supporting Information

The Supporting Information is available free of charge at <https://pubs.acs.org/doi/10.1021/acscchembio.2c00006>.

High-throughput CRISPR screen assay development data; comparisons of assay windows using two different

high-content imagers; primary screen assay layout and hit triaging strategy; hit validation assay results including nanostring gene expression; bacTRAP mouse model; public HSC microarray experiment analysis results; and materials and methods (PDF)

AUTHOR INFORMATION

Corresponding Author

Shan Yu – Takeda Development Center Americas, Inc., San Diego, California 92121, United States; orcid.org/0000-0002-0237-5039; Email: shan.yu@takeda.com

Authors

Matthew Ericson – Takeda Development Center Americas, Inc., San Diego, California 92121, United States
Andrea Fanjul – Takeda Development Center Americas, Inc., San Diego, California 92121, United States
Derek M. Erion – Takeda Pharmaceutical Company Limited, Cambridge, Massachusetts 02139, United States
Maria Paraskevopoulou – Takeda Pharmaceutical Company Limited, Cambridge, Massachusetts 02139, United States
Erin N. Smith – Takeda Development Center Americas, Inc., San Diego, California 92121, United States
Banumathi Cole – HemoShear Therapeutics, Inc., Charlottesville, Virginia 22902, United States
Ryan Feaver – HemoShear Therapeutics, Inc., Charlottesville, Virginia 22902, United States
Corine Holub – Takeda Development Center Americas, Inc., San Diego, California 92121, United States
Narender Gavva – Takeda Development Center Americas, Inc., San Diego, California 92121, United States
Shane R. Horman – Takeda Development Center Americas, Inc., San Diego, California 92121, United States
Jie Huang – Takeda Development Center Americas, Inc., San Diego, California 92121, United States

Complete contact information is available at:

<https://pubs.acs.org/10.1021/acscchembio.2c00006>

Author Contributions

S.Y. and S.R.H. contributed to the experimental interpretation and drafted the manuscript, J.H., A.F., D.M.E., and N.G. provided input on study design and result interpretation, S.Y. designed the high-throughput screening experiments, B.C. and R.F. designed and performed HemoShear liver cell coculture experiments, S.Y. and M.E. performed high-throughput screening experiments, S.Y. performed hit validation studies, M.P. performed public HSC microarray experiment analysis, E.N.S. performed UK Biobank data analysis.

Funding

This study was funded by Takeda Development Center Americas and HemoShear Therapeutics.

Notes

The authors declare the following competing financial interest(s): The authors who were affiliated with Takeda were employees of Takeda during the course of this work, and have real or potential ownership interest in Takeda. The authors who were affiliated with HemoShear were employees of HemoShear during the course of this work, and have real or potential ownership interest in HemoShear. HemoShear Therapeutics received funding from Takeda for partnership in liver disease drug discovery.

ACKNOWLEDGMENTS

We would like to thank our Takeda Pharmaceutical Company Limited's colleagues L. Dick and A. Berger for providing proteasome inhibitors to test in our in vitro experiments.

REFERENCES

- (1) Hirode, G.; Saab, S.; Wong, R. J. Trends in the Burden of Chronic Liver Disease Among Hospitalized US Adults. *JAMA Netw. Open* **2020**, *3*, No. e201997.
- (2) Berumen, J.; Baglieri, J.; Kisseleva, T.; Mekeel, K. *Liver Fibrosis: Pathophysiology and Clinical Implications*; Wiley Interdiscip. Rev. Syst. Biol. Med, 2021; Vol. 13, p e1499.
- (3) O'Rourke, J. M.; Sagar, V. M.; Shah, T.; Shetty, S. Carcinogenesis on the background of liver fibrosis: Implications for the management of hepatocellular cancer. *World J. Gastroenterol.* **2018**, *24*, 4436–4447.
- (4) Zisser, A.; Ipsen, D. H.; Tveden-Nyborg, P. Hepatic Stellate Cell Activation and Inactivation in NASH-Fibrosis-Roles as Putative Treatment Targets? *Biomedicines* **2021**, *9*, 365.
- (5) Roehlen, N.; Crouch, E.; Baumert, T. F. Liver Fibrosis: Mechanistic Concepts and Therapeutic Perspectives. *Cells* **2020**, *9*, 875.
- (6) Cong, M.; Iwaisako, K.; Jiang, C.; Kisseleva, T. Cell signals influencing hepatic fibrosis. *Int. J. Hepatol.* **2012**, *2012*, 158547.
- (7) Pellicoro, A.; Ramachandran, P.; Iredale, J. P.; Fallowfield, J. A. Liver fibrosis and repair: immune regulation of wound healing in a solid organ. *Nat. Rev. Immunol.* **2014**, *14*, 181–194.
- (8) Elpek, G. Ö. Cellular and molecular mechanisms in the pathogenesis of liver fibrosis: An update. *World J. Gastroenterol.* **2014**, *20*, 7260–7276.
- (9) Varga, J.; Pasche, B. Antitransforming growth factor-beta therapy in fibrosis: recent progress and implications for systemic sclerosis. *Curr. Opin. Rheumatol.* **2008**, *20*, 720–728.
- (10) Dewidar, B.; Meyer, C.; Dooley, S.; Meindl-Beinker, A. N. TGF-beta in Hepatic Stellate Cell Activation and Liver Fibrogenesis-Updated. *Cells* **2019**, *8*, 1419.
- (11) Ran, F. A.; Hsu, P. D.; Wright, J.; Agarwala, V.; Scott, D. A.; Zhang, F. Genome engineering using the CRISPR-Cas9 system. *Nat. Protoc.* **2013**, *8*, 2281–2308.
- (12) Wang, T.; Wei, J. J.; Sabatini, D. M.; Lander, E. S. Genetic screens in human cells using the CRISPR-Cas9 system. *Science* **2014**, *343*, 80–84.
- (13) Doench, J. G. Am I ready for CRISPR? A user's guide to genetic screens. *Nat. Rev. Genet.* **2018**, *19*, 67–80.
- (14) Korkut, A.; Zaidi, S.; Kanchi, R. S.; Rao, S.; Gough, N. R.; Schultz, A.; Li, X.; Lorenzi, P. L.; Berger, A. C.; Robertson, G.; et al. A Pan-Cancer Analysis Reveals High-Frequency Genetic Alterations in Mediators of Signaling by the TGF-beta Superfamily. *Cell Syst.* **2018**, *7*, 422–437.
- (15) Yu, H.-x.; Yao, Y.; Bu, F.-t.; Chen, Y.; Wu, Y.-t.; Yang, Y.; Chen, X.; Zhu, Y.; Wang, Q.; Pan, X.-y.; et al. Blockade of YAP alleviates hepatic fibrosis through accelerating apoptosis and reversion of activated hepatic stellate cells. *Mol. Immunol.* **2019**, *107*, 29–40.
- (16) Bourd-Boittin, K.; Le Pabic, H.; Bonnier, D.; L'Helgoualc'h, A.; Th  ret, N. RACK1, a new ADAM12 interacting protein. Contribution to liver fibrogenesis. *J. Biol. Chem.* **2008**, *283*, 26000–26009.
- (17) Atorrasagasti, C.; Aquino, J. B.; Hofman, L.; Alaniz, L.; Malvicini, M.; Garcia, M.; Benedetti, L.; Friedman, S. L.; Podhajcer, O.; Mazzolini, G. SPARC downregulation attenuates the profibrogenic response of hepatic stellate cells induced by TGF-beta1 and PDGF. *Am. J. Physiol.: Gastrointest. Liver Physiol.* **2011**, *300*, G739–G748.
- (18) Sancho, P.; Mainez, J.; Crosas-Molist, E.; Roncero, C.; Fern  ndez-Rodr  guez, C. M.; Pinedo, F.; Huber, H.; Eferl, R.; Mikulits, W.; Fabregat, I. NADPH oxidase NOX4 mediates stellate cell activation and hepatocyte cell death during liver fibrosis development. *PLoS One* **2012**, *7*, No. e45285.
- (19) Mannaerts, I.; Schroyen, B.; Verhulst, S.; Van Lommel, L.; Schuit, F.; Nyssen, M.; van Grunsven, L. A. Gene expression profiling of early hepatic stellate cell activation reveals a role for Igfbp3 in cell migration. *PLoS One* **2013**, *8*, No. e84071.
- (20) Magdaleno, F.; Arriazu, E.; Ruiz de Galarreta, M.; Chen, Y.; Ge, X.; Conde de la Rosa, L.; Nieto, N. Cartilage oligomeric matrix protein participates in the pathogenesis of liver fibrosis. *J. Hepatol.* **2016**, *65*, 963–971.
- (21) Gonz  lez-Fern  ndez, B.; S  nchez, D. I.; Crespo, I.; San-Miguel, B.; Alvarez, M.; Tu  n, M. J.; Gonz  lez-Gallego, J. Inhibition of the SphK1/S1P signaling pathway by melatonin in mice with liver fibrosis and human hepatic stellate cells. *Biofactors* **2017**, *43*, 272–282.
- (22) Chen, W.; Wu, X.; Yan, X.; Xu, A.; Yang, A.; You, H. Multitranscriptome analyses reveal prioritized genes specifically associated with liver fibrosis progression independent of etiology. *Am. J. Physiol.: Gastrointest. Liver Physiol.* **2019**, *316*, G744–G754.
- (23) Wu, J.-C.; Luo, S.-Z.; Liu, T.; Lu, L.-G.; Xu, M.-Y. linc-SCRGI accelerates liver fibrosis by decreasing RNA-binding protein tristetraprolin. *FASEB J.* **2019**, *33*, 2105–2115.
- (24) Luangmonkong, T.; Suriguga, S.; Bigaeva, E.; Boersema, M.; Oosterhuis, D.; de Jong, K. P.; Schuppan, D.; Mutsaers, H. A. M.; Olinga, P. Evaluating the antifibrotic potency of galunisertib in a human ex vivo model of liver fibrosis. *Br. J. Pharmacol.* **2017**, *174*, 3107–3117.
- (25) Hammad, S.; Cavalcanti, E.; Werle, J.; Caruso, M. L.; Dropmann, A.; Ignazzi, A.; Ebert, M. P.; Dooley, S.; Giannelli, G. Galunisertib modifies the liver fibrotic composition in the Abcb4Ko mouse model. *Arch. Toxicol.* **2018**, *92*, 2297–2309.
- (26) Shah, R. A.; Kowdley, K. V. Obeticholic acid for the treatment of nonalcoholic steatohepatitis. *Expert Rev. Gastroenterol. Hepatol.* **2020**, *14*, 311–321.
- (27) Feaver, R. E.; Cole, B. K.; Lawson, M. J.; Hoang, S. A.; Marukian, S.; Blackman, B. R.; Figler, R. A.; Sanyal, A. J.; Wamhoff, B. R.; Dash, A. Development of an in vitro human liver system for interrogating nonalcoholic steatohepatitis. *JCI Insight* **2016**, *1*, No. e90954.
- (28) El Taghdouini, A.; S  rensen, A. L.; Reiner, A. H.; Coll, M.; Verhulst, S.; Mannaerts, I.; Oie, C. I.; Smedsr  d, B.; Najimi, M.; Sokal, E.; et al. Genome-wide analysis of DNA methylation and gene expression patterns in purified, uncultured human liver cells and activated hepatic stellate cells. *Oncotarget* **2015**, *6*, 26729–26745.
- (29) Heiman, M.; Schaefer, A.; Gong, S.; Peterson, J. D.; Day, M.; Ramsey, K. E.; Su  rez-Fari  as, M.; Schwarz, C.; Stephan, D. A.; Surmeier, D. J.; et al. A translational profiling approach for the molecular characterization of CNS cell types. *Cell* **2008**, *135*, 738–748.
- (30) Sauerbruch, T.; Schierwagen, R.; Trebicka, J. Managing portal hypertension in patients with liver cirrhosis. *F1000Research* **2018**, *7*, 533.
- (31) Asrani, S. K.; Devarbhavi, H.; Eaton, J.; Kamath, P. S. Burden of liver diseases in the world. *J. Hepatol.* **2019**, *70*, 151–171.
- (32) Axley, P.; Mudumbi, S.; Sarker, S.; Kuo, Y.-F.; Singal, A. Patients with stage 3 compared to stage 4 liver fibrosis have lower frequency of and longer time to liver disease complications. *PLoS One* **2018**, *13*, No. e0197117.
- (33) Campos-Murgu  a, A.; Rom  n-Calleja, B. M.; Toledo-Coronado, I. V.; Gonz  lez-Regueiro, J. A.; Sol  s-Ortega, A. A.; K  sulas-Delint, D.; Cruz-Conteras, M.; Cruz-Yedra, N.; Cubero, F. J.; Nevzorova, Y. A.; et al. Liver fibrosis in patients with metabolic associated fatty liver disease is a risk factor for adverse outcomes in COVID-19. *Dig. Liver Dis.* **2021**, *53*, 525–533.
- (34) Xiang, F.; Sun, J.; Chen, P.-H.; Han, P.; Zheng, H.; Cai, S.; Kirk, G. D. Early Elevation of Fibrosis-4 Liver Fibrosis Score Is Associated With Adverse Outcomes Among Patients With Coronavirus Disease 2019. *Clin. Infect. Dis.* **2021**, *73*, e594–e601.
- (35) Otogawa, K.; Ogawa, T.; Shiga, R.; Ikeda, K.; Kawada, N. Induction of tropomyosin during hepatic stellate cell activation and the progression of liver fibrosis. *Hepatology* **2009**, *3*, 378–383.

(36) Winkler, I.; Bitter, C.; Winkler, S.; Weichenhan, D.; Thavamani, A.; Hengstler, J. G.; Borkham-Kamphorst, E.; Kohlbacher, O.; Plass, C.; et al. Identification of Ppargamma-modulated miRNA hubs that target the fibrotic tumor microenvironment. *Proc. Natl. Acad. Sci. U. S. A.* **2020**, *117*, 454–463.

(37) Yang, W.; He, H.; Wang, T.; Su, N.; Zhang, F.; Jiang, K.; Zhu, J.; Zhang, C.; Niu, K.; Wang, L.; et al. Single-Cell Transcriptomic Analysis Reveals a Hepatic Stellate Cell-Activation Roadmap and Myofibroblast Origin During Liver Fibrosis in Mice. *Hepatology* **2021**, *74*, 2774–2790.

(38) Pose, E.; Trebicka, J.; Mookerjee, R. P.; Angeli, P.; Ginès, P. Statins: Old drugs as new therapy for liver diseases? *J. Hepatol.* **2019**, *70*, 194–202.

(39) Ciardullo, S.; Perseghin, G. Statin use is associated with lower prevalence of advanced liver fibrosis in patients with type 2 diabetes. *Metabolism* **2021**, *121*, 154752.

(40) Kikuchi, A.; Monga, S. P. PDGFRalpha in liver pathophysiology: emerging roles in development, regeneration, fibrosis, and cancer. *Gene Expression* **2015**, *16*, 109–127.

(41) Bray, M.-A.; Singh, S.; Han, H.; Davis, C. T.; Borgeson, B.; Hartland, C.; Kost-Alimova, M.; Gustafsdottir, S. M.; Gibson, C. C.; Carpenter, A. E. Cell Painting, a high-content image-based assay for morphological profiling using multiplexed fluorescent dyes. *Nat. Protoc.* **2016**, *11*, 1757–1774.

(42) Roti, G.; Stegmaier, K. Genetic and proteomic approaches to identify cancer drug targets. *Br. J. Cancer* **2012**, *106*, 254–261.

(43) Santos, R.; Ursu, O.; Gaulton, A.; Bento, A. P.; Donadi, R. S.; Bologa, C. G.; Karlsson, A.; Al-Lazikani, B.; Hersey, A.; Oprea, T. I.; et al. A comprehensive map of molecular drug targets. *Nat. Rev. Drug Discovery* **2017**, *16*, 19–34.

(44) Fang, H.; Consortium, U.-D.; De Wolf, H.; Knezevic, B.; Burnham, K. L.; Osgood, J.; Sanniti, A.; Lledó Lara, A.; Kasela, S.; De Cesco, S.; et al. A genetics-led approach defines the drug target landscape of 30 immune-related traits. *Nat. Genet.* **2019**, *51*, 1082–1091.

(45) MacNamara, A.; Nakic, N.; Amin Al Olama, A.; Guo, C.; Sieber, K. B.; Hurle, M. R.; Gutteridge, A. Network and pathway expansion of genetic disease associations identifies successful drug targets. *Sci. Rep.* **2020**, *10*, 20970.